JOURNAL OF GEOPHYSICAL RESEARCH, VOL. 103, NO. D13, PAGES 16,575–16,596, JULY 20, 1998

Local closure during the First Aerosol Characterization Experiment (ACE 1): Aerosol mass concentration and scattering and backscattering coefficients

P. K. Quinn and D. J. Coffman

Pacific Marine Environmental Laboratory, NOAA, Seattle, Washington
Joint Institute for the Study of the Atmosphere and Ocean, University of Washington, Seattle

Abstract. The radiative effects of tropospheric aerosol particles are a complex function of the chemical, physical, and optical properties of the aerosol. Closure experiments provide a means for identifying and reducing uncertainties associated with these aerosol properties and hence with the estimation of aerosol radiative forcing. In a closure experiment, an aerosol property is measured by one or more methods and calculated from a model that is based on other independently measured properties. A comparison of the measured and calculated values can reveal inadequacies in either the measurements or the model. A goal of the Aerosol Characterization Experiments (ACE) is to reduce the uncertainty associated with estimating aerosol radiative forcing through both local and column closure experiments. The remote marine aerosol encountered during ACE 1 was well suited for such closure studies because of its relatively simple chemical composition. Local closure experiments were conducted on board the NOAA RV *Discoverer* focusing on the aerosol mass concentration and scattering and backscattering coefficients. Aerosol mass was determined by gravimetric analysis, ion chromatography, and by converting the number size distribution to a mass distribution. Scattering and backscattering coefficients were measured with an integrating nephelometer and calculated from a Mie scattering model. The different measures of mass agreed for both the submicron and supermicron aerosol indicating that within experimental uncertainty, the aerosol was composed entirely of ionic species and associated water mass. Measured and calculated values of scattering and backscattering coefficients for submicron aerosol agreed within experimental uncertainty. There was an offset, however, between the Mie-calculated true values and the measured values that is not explained by nonidealities of the nephelometer response. Closure was not obtained for scattering or backscattering in the supermicron size range due to inadequacies of the techniques used to measure the size distribution and scattering in this size range. Both the mass and the scattering closure experiments indicate a need for an improved understanding of the response of aerosol growth, mixing state, and scattering to changes in relative humidity.

1. Introduction

Tropospheric aerosols pose one of the largest uncertainties in calculating the net shortwave radiative forcing resulting from anthropogenic changes in the composition of the atmosphere [*Intergovernmental Panel on Climate Change (IPCC)*, 1996]. This is due to the many processes (aerosol formation, growth, and removal) and parameters (aerosol chemical, physical, and optical properties) that define an aerosol system. The flux of solar radiation that is redirected back to space due to scattering by tropospheric aerosol is proportional to the fraction of radiation scattered upward by the aerosol averaged over the sunward hemisphere ($\overline{\beta}$), the aerosol mass scattering efficiency (α_{sp}), and the column burden of the aerosol (B) such that

$$\Delta F \propto \overline{\beta}\alpha_{sp} f_{sp}(\mathrm{RH}) B \quad (1)$$

where $f_{sp}(\mathrm{RH})$ takes into account the dependence of scattering by the aerosol on relative humidity. Here the aerosol mass scattering efficiency is defined for an individual chemical component j as the change in scattering by the aerosol per change in mass increment of component j or

$$\alpha_{sp,j} = \frac{\partial \sigma_{sp}}{\partial m_j} \quad (2)$$

Paper number 97JD03757.
0148-0227/98/97JD-03757$09.00

Determination of component mass scattering efficiencies relies on measurements of the scattering coefficient and component mass concentrations. The upscatter fraction $\overline{\beta}$ can be inferred from measurable quantities including the hemispheric backscatter fraction, b, which is equal to the hemispheric backscattering coefficient, σ_{bsp}, divided by the scattering coefficient, σ_{sp} [*Wiscombe and Grams,* 1976; *Marshall et al.,* 1995]. Hence reducing the uncertainty in the estimation of aerosol radiative forcing depends, in part, on reducing the uncertainty associated with the aerosol mass concentration, scattering coefficient, and backscattering coefficient.

Closure experiments provide one approach for identifying and reducing the uncertainties associated with these parameters. A closure experiment requires an over-determined set of observations such that the measured value of an important system property can be compared to a value calculated with an appropriate model based on independent measurements. The measured and calculated values of the variable then are compared. Prior to performing a closure experiment, the uncertainties of the measurements and models must be well quantified, and the level of uncertainty that is acceptable must be known. Closure is achieved if there is agreement between the measured and theoretical values within the accepted level of uncertainty. This agreement indicates that both the measurements and the model offer a suitable representation of the observed system. Poor agreement indicates that there are problems in the measurements and/or models that need to be identified and corrected.

Performing mass and scattering closure experiments on the same data set is a natural course of action as many aerosol properties are common to both. For example, measured number and chemical mass size distributions can be used to derive the total aerosol mass concentration. They also can be used in a scattering closure experiment to calculate scattering and backscattering coefficients. Therefore the achievement of mass closure instills confidence in the use of these properties in a scattering closure experiment.

During the First Aerosol Characterization Experiment (ACE 1), simultaneous measurements of aerosol chemical, physical, and optical properties were made on board the NOAA RV *Discoverer* allowing for local closure studies focused on the aerosol mass concentration, scattering coefficient, and backscattering coefficient. Three methods were used to determine the aerosol mass concentration (Figure 1). Concentrations of total aerosol mass were determined from gravimetric analysis and by converting the measured number size distribution to a mass distribution using densities es-

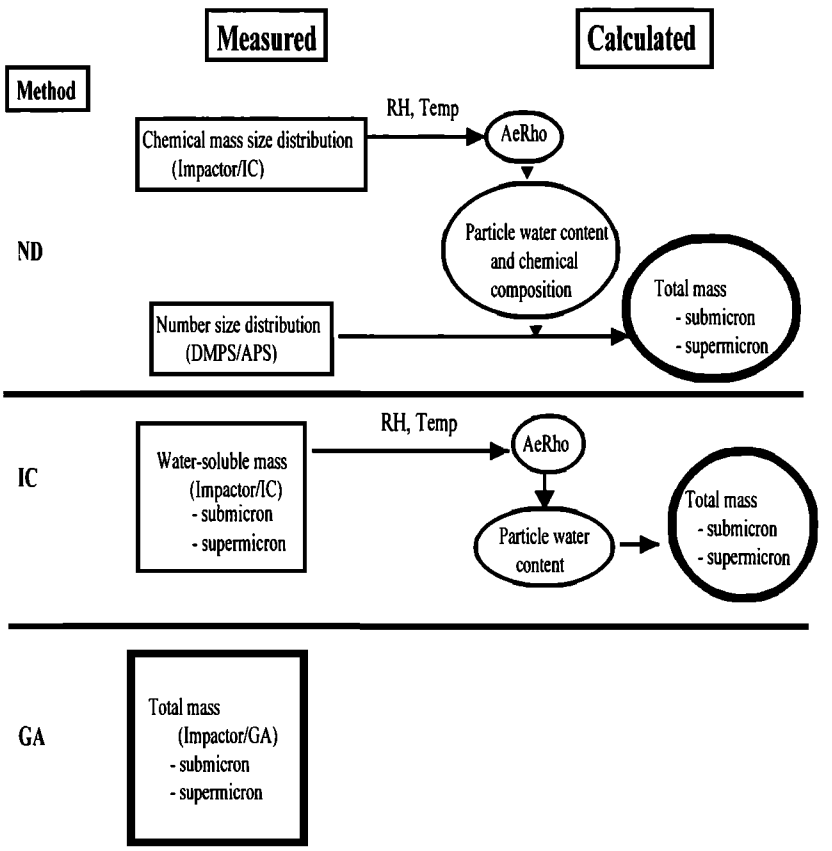

Figure 1. Design of the mass closure experiment. The three methods used to estimate the aerosol mass concentration are shown. Measured and calculated properties are in rectangles and circles, respectively. The quantities from each method to be compared, submicron and supermicron mass, are indicated by heavy borders. ND, mass derived from the number distribution; IC, mass derived from the ion chromatography analysis; GA, mass derived from the gravimetric analysis.

timated from the measured chemical composition coupled with a chemical equilibrium model. In addition, the concentration of water-soluble ionic species was determined from ion chromatography.

For the scattering closure experiment, aerosol scattering and backscattering coefficients were measured directly using an integrating nephelometer (Figure 2). They also were calculated from a Mie scattering model coupled with measured number and chemical mass size distributions. In addition, the model was modified to simulate the nephelometer response for the determination of nephelometer-simulated scattering and backscattering coefficients.

Presented here are details of the measurement and calculation methods used in the closure experiments. Known sources of error associated with each method are identified and quantified. The results of the closure experiments are presented in the context of these uncertainties to ascertain whether or not closure was achieved. In those instances where closure was not obtained, improvements to the methods are suggested with the goal of reducing the uncertainty of the measured or calculated parameter. An analysis of the aerosol optical properties during ACE 1 based on measured chemical and physical properties is presented in a companion paper by *Quinn et al.* [this issue].

2. Experimental Design

The closure experiments described here were based on four independent measurement techniques: multijet cascade impactors, a differential mobility particle sizer (DMPS), an aerodynamic particle sizer (APS), and an integrating nephelometer. To reduce the possibility of systematic differences in the measurements, all aerosol instruments sampled from a common inlet. Attempts were made to maintain isokinetic flow and minimize the loss of supermicron particles by rotating the inlet into the relative wind. The inlet was rotated manually until it was aligned with an anemometer mounted 0.5 m above it. Air entered the inlet through a 5 cm diameter hole, passed through an expansion cone, and then into

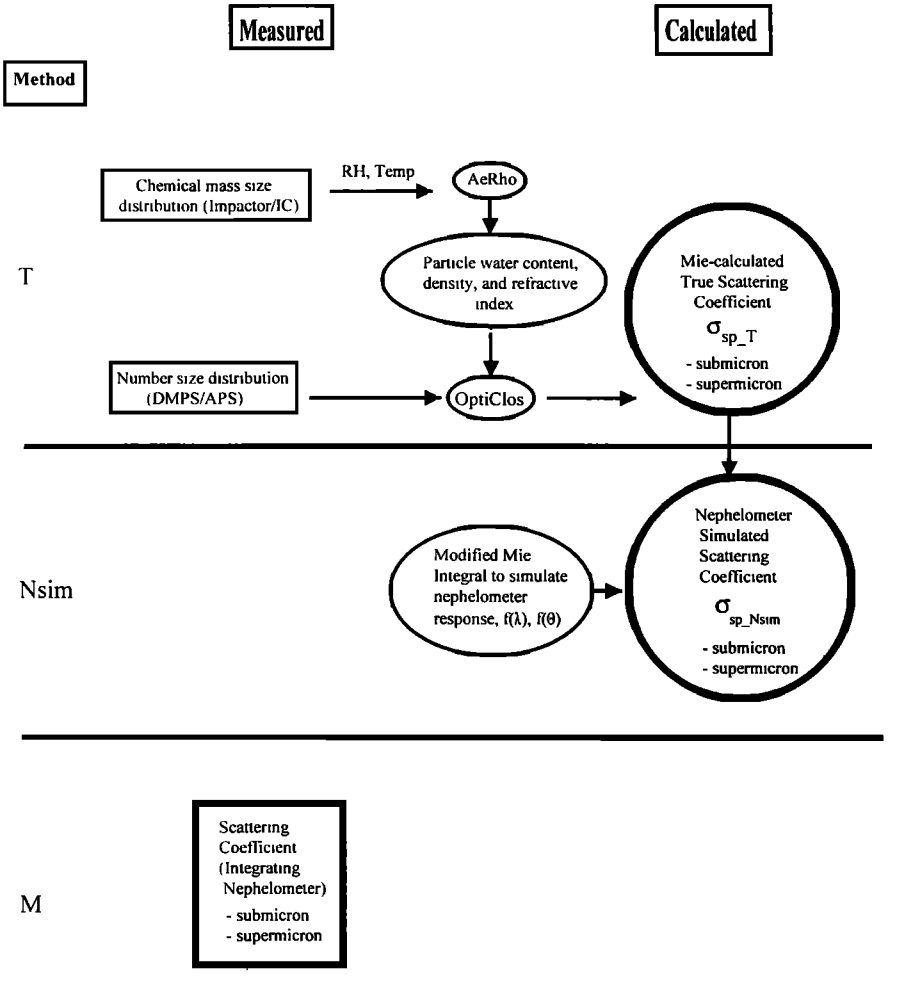

Figure 2. Design of the scattering closure experiment. Measured and calculated properties are shown in rectangles and circles, respectively. The compared quantities derived from each method, submicron and supermicron scattering coefficients, are indicated by heavy borders. The same design was used for the backscattering closure experiment. T, Mie-calculated true scattering; Nsim, Mie calculation of the scattering modified to simulate the nephelometer response; M, scattering measured by the integrating nephelometer.

the 20 cm diameter sampling mast that had a length of 6 m. The flow through the mast was 1 m^3 min^{-1}. The last 1.5 m of the mast were heated to establish a low reference relative humidity (RH) for the sample air of 30 to 45% (hereafter referred to as the instrumental RH). Individual 1.9 cm diameter stainless steel tubes extended into the heated portion of the mast. These were connected to the various aerosol instruments with carbon-embedded conductive tubing to prevent the loss of small diameter particles through static charging.

2.1. Mass Closure Experiment

2.1.1. Gravimetric analysis (GA). Submicron and supermicron aerosol mass concentrations were estimated using three techniques. (The submicron and supermicron size fractions referred to here and throughout the paper are in terms of aerodynamic diameter, D_{aero}. To reference them to geometric diameters, for a particle density of 1.7 g cm^{-3}, D_{aero} of 1.0 μm is equal to a geometric diameter of 0.81 μm, and D_{aero} of 10 μm is equal to a geometric diameter of 7.7 μm.) The most direct method involved the gravimetric analysis of samples collected with a multijet cascade impactor having two size cuts: 50% aerodynamic cutoff diameters, $D_{50,aero}$ = 1.0 μm and $D_{50,aero}$ = 10 μm [*Berner et al.*, 1979]. A 47-mm Millipore Fluoropore filter (1.0-μm pore size) was used for the submicron stage and a 90-mm Tedlar impactor film was used for the supermicron stage. A grease cup ($D_{50,aero}$ = 12 μm) at the inlet of the impactor was covered with silicone grease to prevent the bounce of large particles onto the downstream stages. All handling of the substrates was done in a glove box that was purged continuously with room air that had passed through a scrubber containing potassium carbonate and citric acid for the removal of acidic and basic gases.

Filters and films were weighed at the Pacific Marine Environmental Laboratory (PMEL) before and after sample collection with a Mettler UMT2 and Cahn Model 29 microbalance, respectively. The microbalances were housed in a glove box kept at a humidity of 33 ± 2%. Room air was passed through a scrubber of activated charcoal, potassium carbonate, and citric acid to remove gas phase organics, acids, and ammonia. To maintain a constant RH, the scrubbed air was circulated through a flat baffle box containing a saturated solution of $MgCl_2 \cdot 6H_2O$ and then through the glove box [*Young*, 1967; *McInnes et al.*, 1996]. Static charging, which can result in balance instabilities, was minimized by coating the walls of the glove box with a static dissipative polymer (Tech Spray, Inc.), placing an antistatic mat on the glove box floor, using antistatic gloves while handling the substrates, and exposing the substrates to a ^{210}Po source to dissipate any charge that had built up on the substrates.

Balance accuracy was checked every tenth sample with calibration weights. The standard deviation (1σ) of the weighing procedure was determined from repetitive weighings of the same substrate and found to be ±2 μg for the Fluoropore filters and ±6 μg for the Tedlar films. On average, these values are ±4% and ±2% of the total sample mass for the filters and films, respectively. Before and after sample collection, substrates were stored double-bagged with the outer bag containing citric acid to prevent absorption of gas phase ammonia. Previous studies using the same collection, storage, and weighing techniques have shown that the filter material maintains a near-constant weight between sample collection and the final weighing [*McInnes et al.*, 1996].

Maintaining the glove box at a constant 33% RH allows each sampled substrate to come into equilibrium with the same vapor pressure of water thus reducing experimental uncertainty due to a variable laboratory RH. The resulting mass concentrations from the GA include the water mass that is associated with the aerosol at 33% RH. Additional water mass may also be present due to interactions between the collected aerosol and the sampling substrate. The response of particles collected on a filter to changes in RH has been shown to be different than that of individual particles or bulk solutions of similar chemical composition [*McInnes et al.*, 1996].

2.1.2. Ion chromatography analysis (IC). The second independent method in the mass closure experiment involved determining the concentration of water-soluble ionic species collected with an impactor having two size cuts ($D_{50,aero}$ = 1.0 μm and $D_{50,aero}$ = 10 μm). The same substrates were used as for the GA and were analyzed by ion chromatography for Na^+, NH_4^+, K^+, Mg^{2+}, Ca^{2+}, Cl^-, Br^-, NO_3^-, $SO_4^=$, and MSA^- [*Quinn et al.*, 1995; this issue].

Blank levels were determined by loading an impactor with substrates and deploying it at the sampling site for the length of a typical sampling period without drawing any air through it. On average, the blank to sample ratios were as follows: Na^+ = 17%, NH_4^+ = 40%, K^+ = 30%, Mg^{2+} = 18%, Ca^{2+} = 60%, Cl^- = 20%, Br^- = 25%, NO_3^- = 40%, and $SO_4^=$ = 9%. MSA^- blanks were below detection limit.

The amount of water associated with the aerosol at the instrumental RH (30 to 45%) (as determined by AeRho, a chemical model based on thermodynamic equilibrium (see section 2.1.4)) was added to the IC mass concentrations for both the submicron and supermicron aerosol size ranges.

2.1.3. Mass derived from the number distribution (ND). The third method for the estimation of the aerosol mass concentration involved converting the measured number size distribution to a mass size distribution. The number size distribution between 0.02 and 0.57 μm was measured every 10 min with a DMPS at an RH of 10%. The mobility distribution from the DMPS was inverted to a number distribution by assuming that a Fuchs-Boltzman charge distribution resulted from the Kr^{85} charge neutralizer (model 3077, TSI, Inc.). The data were corrected for diffusional losses [*Covert et al.*,

1997] and size dependent counting efficiencies [*Wiedensohler et al.*, 1997].

The number distribution between 0.85 and 9.6 μm was measured with an APS at the instrumental RH of 30 to 45%. Data for aerodynamic diameters greater than 5 μm were discarded, however, due to interference from phantom counts. The APS diameters were converted to geometric diameters by dividing by the square root of the particle density. Densities were calculated from the chemical equilibrium model AeRho. To align the DMPS and APS size distributions, DMPS diameters were grown to the RH of the air sampled by the APS using growth factors derived from humidity-controlled tandem differential mobility analyzer (H-TDMA) measurements [*Berg et al.*, this issue]. The H-TDMA measurements were made at a range of particle diameters up to 0.2 μm, hence they are applicable to the submicron size range. A value of 1.2 was used for the non-sea-salt (nss) sulfate aerosol and 1.5 for the sea-salt aerosol. The assumption of constant growth factors for each aerosol type is reasonable as they were found to vary by only $\pm$5% over the course of the experiment.

An interactive routine was used to fit lognormal curves to the different modes of the size distribution. This allows for the calculation of optical properties for each mode. It was done here so that the scattering and backscattering due to the accumulation and coarse modes could be determined. To achieve the best results for the entire size range (0.02 to 5 μm), the number distribution was converted to a surface area distribution, and the fit was performed on the surface area distribution. The fitting routine is based on the DISTFIT model of *Whitby and Whitby* [1989]. It is more interactive than DISTFIT, however, in that the user can specify the number of possible modes and can select the minimum diameter between each mode.

A single lognormal curve was sufficient to characterize the mean diameter and geometric standard deviation of the Aitken mode (0.02 to 0.08 μm diameter) and the accumulation mode (0.08 to 0.50 μm). The coarse aerosol, however, was fit with two lognormal modes to accommodate either a bimodal or a skewed structure. A comparison of three fitting techniques for the coarse aerosol is shown in Figure 3. One technique uses one mode and optimizes the fit in terms of total surface area. A second also uses one mode but optimizes for the modal diameter. The third is a two-mode fit and results in the best representation of both the total surface area concentration and mean diameter of the coarse aerosol. This follows *O'Dowd et al.* [1997] who suggest that different production mechanisms generate several modes within the coarse size fraction.

Finally, the lognormally fit surface area size distribution was converted to a volume size distribution. The size-dependent particle densities estimated from AeRho were used to convert the volume size distribution to a mass size distribution. The resulting mass concentrations were summed to produce integral values for the submicron and supermicron size ranges. Mass estimates derived from the number size distribution include the amount of water associated with the aerosol at instrumental RH.

2.1.4. Calculation of the aerosol water mass and density. The water mass associated with the

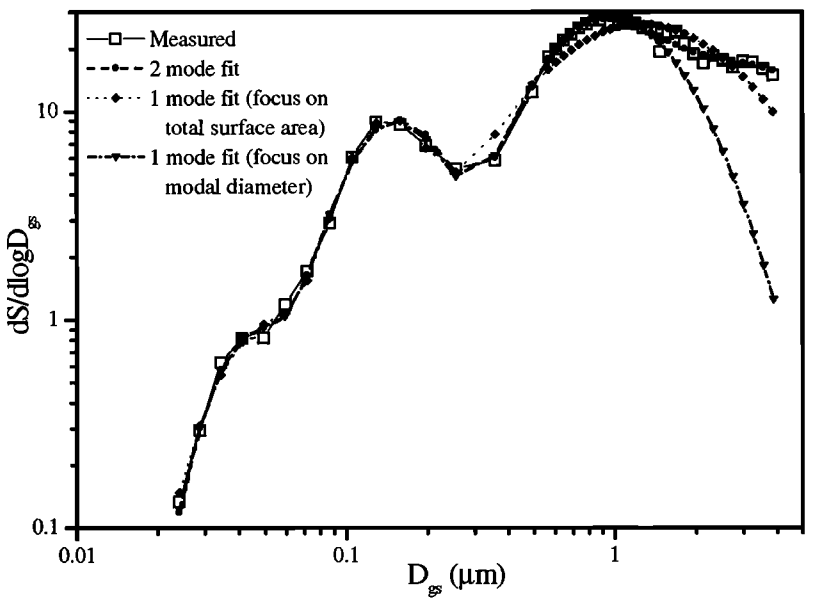

Figure 3. A comparison of three fitting techniques for the coarse aerosol surface area size distribution. The techniques include a two-mode fit that uses two lognormal curves to best represent both the modal mean diameter and total surface area concentration, a one-mode fit that uses one lognormal curve and optimizes the fit in terms of surface area, and a one-mode fit that uses one lognormal curve and optimizes the fit in terms of the modal diameter.

aerosol and the particle density at the instrumental RH of 30 to 45% were estimated as a function of size from AeRho, a chemical model based on thermodynamic equilibrium. As used in this application, AeRho is a static model. It is designed to take the measured ionic composition of the aerosol and the constant sampling RH and to determine the molecular composition of the chemical species within the aerosol. The molecular composition then is used to calculate the water mass associated with the aerosol and the aerosol density. The model is not used to describe a dynamic system in which changes in the concentration of gas phase species affect the aerosol molecular composition. Therefore the model does not include interactions between the gas and aqueous phases. In addition, because of the constant sampling RH, it is not necessary to take into account changes in particle size with changes in RH.

To simplify the model calculations, the aerosol was assumed to be an external mixture of nss sulfate and sea-salt aerosol. Although this simplifies the calculations, it may limit their accuracy as the analysis of single particles by microscopic and mass spectrometric techniques suggests the aerosol was internally mixed to some degree [*Murphy et al.*, 1997]. Consequences of this assumption will be discussed throughout the paper.

The nss sulfate aerosol is composed of $SO_4^=$, NH_4^+, and H_2O, and the sea-salt aerosol is composed of Na^+, Cl^-, sea-salt $SO_4^=$, and H_2O. The chemical reactions allowed to occur are shown in Table 1. Data from a seven-stage multijet cascade impactor were used as model input. Specifically, this included the measured concentrations of $SO_4^=$, NH_4^+, Na^+, and Cl^- within each impactor stage. The seven-stage impactor samples were collected over the same time periods as the two-stage impactors discussed above. The use of the seven-stage data as model input allows for chemical information with greater size resolution, while the use of two-stage impactors for gravimetric analysis allows for mass information with greater time resolution. The submicron and supermicron water-soluble ionic mass collected on the two-stage and seven-stage impactors agreed within experimental uncertainty.

The ionic molalities for each of the input species are determined initially by assuming that the activity of water is equal to the instrumental RH. Then, using the ZSR method [*Zdanovskii*, 1936; *Robinson and Stokes*, 1965], a further approximation of the water content of the aerosol is made. Aqueous phase concentrations are activity corrected using the method of *Bromley* [1973] which allows for the prediction of activity coefficients of strong electrolytes in multielectrolyte solutions based on binary solution activity coefficients [*Pilinis and Seinfeld*, 1987; *Quinn et al.*, 1992]. The pure-solution binary activity coefficients are calculated using the method of *Pitzer and Mayorga* [1973]. The ionic species are partitioned between the solid and aqueous phases with the solids precipitating in the most thermodynamically favorable order. The crystallization RH used for each solid phase species is listed in Table 1. The remaining aqueous ionic species are converted to aqueous compounds in accordance with the thermodynamic equilibrium constants. Finally, thermodynamic equilibrium

Table 1. Chemical Reactions Included in AeRho, the Thermodynamic Chemical Equilibrium Model of the nss Sulfate/Sea-Salt Aerosol System, Which Was Used to Calculate the Aerosol Density and Refractive Index for Each Impactor Size Bin

	Crystallization RH, %
Aqueous Reactions	
Na_2SO_4 (aq) $\leftrightarrow$ $2Na^+$ (aq) + $SO_4^=$ (aq)	
NH_4HSO_4 (aq) $\leftrightarrow$ NH_4^+ (aq) + HSO_4^- (aq)	
$(NH_4)_2SO_4$ (aq) $\leftrightarrow$ $2NH_4^+$ (aq) + $SO_4^=$ (aq)	
$NaHSO_4$ (aq) $\leftrightarrow$ Na^+ (aq) + HSO_4^- (aq)	
HCl (aq) $\leftrightarrow$ H^+ (aq) + Cl^- (aq)	
NH_4Cl (aq) $\leftrightarrow$ NH_4^+ (aq) + Cl^- (aq)	
NaCl (aq) $\leftrightarrow$ Na^+ (aq) + Cl^- (aq)	
H_2SO_4 (aq) $\leftrightarrow$ HSO_4^- (aq) + H^+ (aq)	
HSO_4^- (aq) $\leftrightarrow$ H^+ (aq) + $SO_4^=$ (aq)	
Solid Phase Reactions	
Na_2SO_4 (s) $\leftrightarrow$ $2Na^+$ (aq) + $SO_4^=$ (aq)	59
$(NH_4)_2SO_4$ (s) $\leftrightarrow$ $2NH_4^+$ (aq) + $SO_4^=$ (aq)	40
NH_4Cl (s) $\leftrightarrow$ NH_4^+ (aq) + Cl^- (aq)	40
NaCl (s) $\leftrightarrow$ Na^+ (aq) + Cl^- (aq)	25
$NaHSO_4$ (s) $\leftrightarrow$ Na^+ (aq) + HSO_4^- (aq)	22

Crystallization RH values were taken from *Tang and Munkelwitz* [1994] except that of NaCl which is based on laboratory studies.

with respect to water is tested for, and the water activity is iterated until equilibrium is established.

By assuming thermodynamic equilibrium, AeRho is able to provide the molecular composition necessary for estimating particle density as a function of particle size. Measurements have shown, however, that metastable particles can exist in the atmosphere [*Rood et al.*, 1989]. Therefore polynomial fits based on data of *Tang and Munkelwitz* [1991, 1994] for metastable particles are used to estimate densities of individual species. Data from *Bray* [1970] are used to estimate the density of H_2SO_4. A volume-weighted average is taken of the density of the individual species to estimate the density of each impactor size bin.

2.2. Scattering and Backscattering Closure Experiment

2.2.1. Measurement of aerosol scattering and backscattering coefficients (M). Measurements of the aerosol scattering and backscattering coefficients were made with an integrating nephelometer (model 3563, TSI, Inc.) at wavelengths of 0.45, 0.55, and 0.7 μm. Results are reported here for the 0.55 μm channel and the instrumental RH of 30 to 45%. The nephelometer-measured scattering and backscattering coefficients are referred to throughout the paper as σ_{sp_M} and σ_{bsp_M}, respectively. Two 1-stage multijet cascade impactors, one having a $D_{50,aero}$ of 1.0 μm and the other 10 μm, were placed upstream of the nephelometer. A grease cup ($D_{50,aero} = 12$ μm) at the inlet of each impactor was covered with silicone grease to prevent bouncing of large particles. In addition, Tedlar films were sprayed with Silicone lubricant and placed on the 1.0 and 10 μm jet plates. A valve switched between the two impactors every 15 min so that sampling alternated between submicron aerosol and all aerosol with $D_{aero} < 10$ μm. The supermicron scattering and backscattering coefficients were calculated by difference. The nephelometer was calibrated with CO_2 at the beginning and end of the experiment and zeroed on a weekly basis throughout the experiment [*Anderson et al.*, 1996].

2.2.2. Calculation of aerosol scattering and backscattering coefficients (T and Nsim). The OptiClos model was used to calculate a scattering (and backscattering) size distribution for the diameter range 0.02 to 5 μm. For input, the model used the fitted size distributions and the refractive index calculated by AeRho. First, the model assigned a chemical composition to each mode of the size distribution. The Aitken and accumulation modes were assumed to be composed of nss $SO_4^=$ aerosol consisting of nss $SO_4^=$ and NH_4^+, and the coarse mode was assumed to be composed of sea salt consisting of Na^+, Cl^-, and sea-salt $SO_4^=$. All modes contained associated water mass, as calculated by AeRho, at the instrumental RH of 30 to 45%.

Using the method of partial molar refraction [*Stelson*, 1990], the particle refractive index as a function of size was derived from AeRho (section 2.1.4). Measured concentrations of $SO_4^=$, NH_4^+, Na^+, and Cl^- from the seven-stage impactor data were used as input. Assuming an external mixture of nss sulfate and sea-salt aerosol, the refractive index for each impactor size bin was calculated. From these data, each size bin of the fitted size distribution was assigned a refractive index. In regions where the lognormal curves of the accumulation and coarse modes overlapped, a weighted average of the nss $SO_4^=$ and sea-salt refractive indices was applied. The modeling scheme that combines the use of AeRho and OptiClos is shown in Figure 4.

The scattering intensity function $|S(\theta, x, n)|^2$ was derived from Mie theory for scattering angle θ, size parameter $x = \pi D_p/\lambda$, wavelength $\lambda = 0.55$ μm, and particle refractive index n. Integrating over angle yields the "true" single-particle scattering efficiency Q_{sp_T} [*Bohren and Huffman*, 1983]

$$Q_{sp\_T}(\lambda, n, D_p) = \frac{1}{x^2}\int_0^{\pi} |S(\theta, x, n)|^2 \sin\theta d\theta. \quad (3)$$

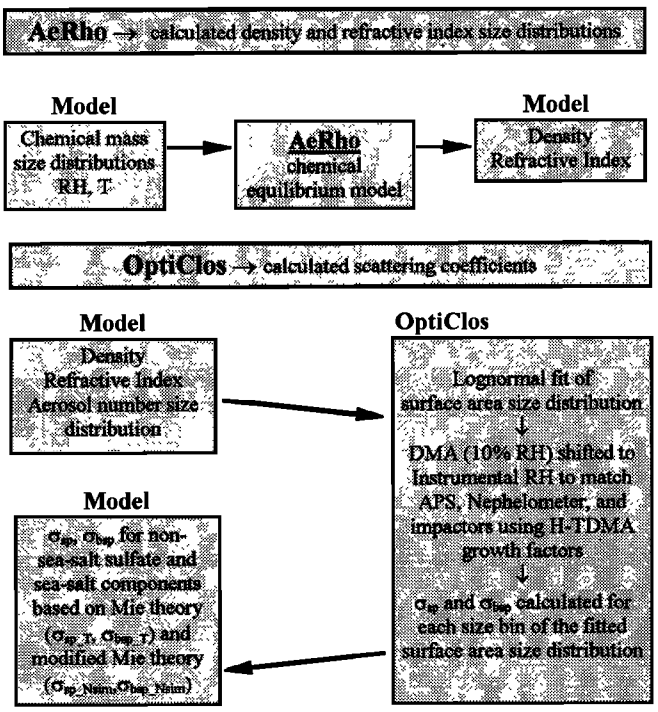

Figure 4. Steps in the chemical thermodynamic equilibrium model, AeRho, used to calculate particle water content, density, and refractive index as a function of size and the Mie scattering model, OptiClos, used to calculate scattering and backscattering coefficients of the aerosol chemical components. An unmodified Mie integral was used to calculate the true scattering (σ_{sp_T}) and backscattering (σ_{bsp_T}) coefficients. A Mie integral modified to simulate the nephelometer response was used to calculate nephelometer-simulated values of σ_{sp_Nsim} and σ_{bsp_Nsim}.

The true scattering coefficient, denoted here by σ_{sp_T}, is obtained by multiplying by the particle cross-sectional area and integrating over the particle size distribution

$$\sigma_{sp\_T}(\lambda, n, N(D_p)) = \int_0^\infty Q_{sp\_T}(\lambda, n, D_p)\frac{\pi D^2}{4}\frac{\partial N}{\partial \log D_p} d\log D_p \quad (4)$$

This property is not measured by the nephelometer, however, due to the instrument's nonlambertian light source, wavelength nonidealities, and truncation of integration angles. Therefore a Mie integral modified to simulate the nephelometer response was used to calculate the simulated nephelometer single-particle scattering efficiency, Q_{sp_Nsim},

$$Q_{sp\_Nsim}(\lambda, n, D_p) = \int_0^\infty \frac{1}{x^2}\int_0^\pi |S(\theta, x, n)|^2 f(\theta) d\theta f(\lambda) d\lambda \quad (5)$$

Measured sensitivity functions were used in (5) such that the angular sensitivity function, $f(\theta)$, replaced $\sin\theta$ to account for the truncation of integration angles, and the wavelength sensitivity function $f(\lambda)$ was inserted to account for wavelength nonidealities [*Heintzenberg*, 1978; *Anderson et al.*, 1996]. The simulated nephelometer scattering coefficient, denoted by σ_{sp_Nsim}, then was calculated from

$$\sigma_{sp\_Nsim}(\lambda, n, N(D_p)) = \int_0^\infty Q_{sp\_Nsim}(\lambda, n, D_p)\frac{\pi D^2}{4}\frac{\partial N}{\partial \log D_p} d\log D_p \quad (6)$$

The scattering (backscattering) coefficients were summed to produce integral values for the accumulation and coarse modes. Through a similar summation process, integral values were calculated for the submicron and supermicron size fractions.

3. Uncertainty Analysis

Assessing whether or not closure is achieved with respect to an aerosol property requires a knowledge of the experimental uncertainty. To test for closure, the relative difference between independently derived values of the same property are compared to the experimental uncertainty. If the difference is within the experimental uncertainty, closure was achieved. If it is outside of the experimental uncertainty, sources of error are identified, and methods for their reduction are pursued.

The determination of aerosol property y_{Mi} by method M_i depends on several parameters p_i with each parameter contributing to the uncertainty of y_{Mi}. The total relative uncertainty of y_{Mi}, $\delta y_{Mi} = \Delta y_{Mi}/y_{Mi}$, is given in terms of the partial derivative of y_{Mi} with respect to each parameter, $\delta y_{Mi}/\delta p_i$, such that

$$\delta y_{Mi}^2 = \sum_i \left(\frac{\delta y_{Mi}}{\delta p_i}\delta p_i\right)^2 \quad (7)$$

Here δp_i is the relative uncertainty of parameter p_i and is given by

$$\delta p_i = \frac{\Delta p_i}{p_i} \quad (8)$$

Equation (7) assumes that all parameters are independent. The total relative uncertainty of a closure study which involves at least two methods to determine y is a combination of the uncertainty of each M_i and can be estimated from the quadratic sum over all δy_{Mi} such that

$$\delta y^2 = \sum_{Mi} (\delta y_{Mi})^2 \quad (9)$$

The uncertainty of aerosol properties determined by measurement was estimated from (7) with the assumption that all parameters contributing to the uncertainty of y_{Mi} were independent. This assumption is not necessarily appropriate for modeled properties, however, as the parameters may not behave independently as they are propagated through the model. Therefore the uncertainty of the calculated properties (mass concentration from ND as well as calculated scattering and backscattering coefficients) was estimated through a series of sensitivity studies described in section 3.2.

3.1. Uncertainty Analysis for the Mass Closure Experiment

Sources of uncertainty and their magnitudes are listed in Table 2 for each method (GA, IC, and ND) used in the mass closure experiment. Values are based on a submicron aerosol mass concentration of 1.0 μg m^{-3} (or 45 μg per 45 m^{-3} of air) and a supermicron concentration of 10 μg m^{-3} (or 450 μg per 45 m^{-3} of air). The total uncertainty for each method was calculated according to (7) and may be an underestimate if the parameters involved are not independent.

For the GA, the relative uncertainty associated with the weighing procedure was based on the standard deviation (1σ) of replicate weighings of either the Millipore filter or Tedlar film. The uncertainty associated with substrate storage and handling was based on a mass change with storage of +4 μg as measured by *McInnes et al.* [1996]. The uncertainty in the RH of the glove box was based on variations in the humidity over the course of weighing the ACE 1 substrates and from the accuracy of the RH sensor (Vaisala, model HMP 233). An uncertainty for inlet losses of larger particles was included in the determination of the supermicron mass concentration for all three methods (GA, IC, ND). The inlet was designed to minimize particle losses by maintaining isokinetic flow as the sampled particles traveled from the atmosphere into the inlet. For practical reasons, it was possible to maintain isokinetic flow for only a range of relative wind speeds encountered (where relative refers to the wind speed resulting from the ship's speed and the true wind speed). Based on the velocity of the sampled air through the inlet and the range of relative wind speeds encountered, particle losses within

Table 2. Sources of Uncertainty in the Mass Closure Experiment

Method, M_i	Parameter, p_i	δp_i,[a] %	δy_{M_i},[b] %
Gravimetric analysis			
Submicron mass[c]	weighing	±4.4	±25
	substrate storage and handling	±8.9	
	RH of glove box	±6.0	
	air volume	±5.0	
Supermicron mass[d]	weighing	±1.3	−16, +26
	substrate storage and handling	±1.0	
	RH of glove box	±6.0	
	inlet losses	+10.0	
	air volume	±5.0	
Ionic analysis			
Submicron mass	IC analysis (includes IC analysis and extraction)	±7.2	±23
	extraction liquid volume	±3.3	
	air volume	±5.0	
	water mass at instrumental RH includes	−21, +23	
	chemical composition[e]	±5.5	
	RH and T[f]	−20, +22	
Supermicron mass	IC analysis (includes IC analysis and extraction)	±7.2	±23
	extraction liquid volume	±3.3	
	inlet losses	+10.0	
	air volume	±5.0	
	water mass at instrumental RH includes	±20.0	
	chemical composition[e]	±4.5	
	RH and T[f]	±20.0	
Derivation from number			
Submicron mass	instrumental sizing	±2.5	−23, +29
	instrumental counting	±10.0	
	conversion of number to mass distribution which includes	−21, +27	
	chemical composition[e]	±0.3	
	RH and T[f]	−17, +21	
	growth factor[g]	−12, +17	
Supermicron mass	instrumental sizing	negligible	−13, +20
	instrumental counting	±1.0	
	conversion of number to mass distribution which includes	−13, +2	
	chemical composition[e]	−0.04, +0.5	
	RH[f]	−13, +0.04	
	growth factor[g]	−1.3, +1.8	
	inlet losses	+20	

[a]Relative uncertainty of parameter p_i as defined by equation (8).

[b]Total relative uncertainty associated with method M_i calculated from equation (7). Sources of error are assumed to be independent. As such, the total error may be an underestimate.

[c]Based on a submicron aerosol mass concentration of 1 μg m^{-3}.

[d]Based on a supermicron aerosol mass concentration of 10 μg m^{-3}.

[e]Chemical composition varied by 2% per chemical species per stage.

[f]RH varied by ±20% and temperature by ±10%.

[g]Growth factor varied by 1.2 ± 5% for nss $SO_4^=$ and 1.5 ± 5% for sea-salt aerosol [*Berg et al.*, this issue].

the supermicron size range were, at most, 10% of the total mass in this size range.

For mass determined by IC, the concentrations of 10 ions (Na^+, NH_4^+, K^+, Mg^{2+}, Ca^{2+}, Cl^-, Br^-, NO_3^-, $SO_4^=$, and MSA^-) were summed to obtain the total concentration of water-soluble ionic species. The overall uncertainty was obtained by using (7) to combine the uncertainty associated with the extraction and analysis of each ion as well as the volume of the sample air. The uncertainty of the water mass concentration was based on a sensitivity analysis in which chemical composition, RH, and T were varied. The sensitivity analysis is described in detail in section 3.2.

Uncertainties in the mass concentrations derived from the ND result from instrumental errors of particle sizing and counting due to flow irregularites in the DMPS and APS and from factors involved in converting the number distribution to a mass distribution. Instrumental systematic errors in sizing and counting were considered to be proportional to the errors in the sheath and sample flows, respectively, of the DMPS and APS [*Marshall,* 1994]. Factors affecting the accuracy of the conversion of the number to a mass size distribution include the aerosol chemical composition, RH, and T of the sampled air stream, and aerosol growth factors. The uncertainty of the conversion was based on a sensitivity analysis in which each of these factors was varied independently. Results of the sensitivity analysis are presented in section 3.2. An additional uncertainty for supermicron particles was taken into account resulting from the truncation of the APS data at 5 μm. Up to 10% of the supermicron mass was assumed to be lost based on the amount collected on the largest stage of the seven-stage impactor ($4.7 \leq D_{p,\mathrm{aero}} < 10\,\mu\mathrm{m}$). This was added to the 10% inlet loss for a total loss of 20%.

3.2. Uncertainty Analysis for the Scattering and Backscattering Closure Experiment

Sources of uncertainty and their magnitudes are listed in Table 3 for the methods used in the scattering and backscattering closure experiments. The total uncertainty for each method was calculated according to (7).

Sources of uncertainties associated with the use of the integrating nephelometer include photon counting during measurement, zeroing, and calibration, literature values of calibration gas scattering coefficients, and variations in gas density within the nephelometer. Values for these uncertainties were based on *Anderson et al.* [1996] and assumed scattering and backscattering levels of 20 and 2 Mm^{-1}, respectively. The uncertainty of the RH of the sampled air stream was based on variations in the humidity throughout ACE 1 and the accuracy of the RH sensor (Vaisala, model HMP 233). The uncertainty of the $D_{50,\mathrm{aero}}$ values of the upstream impactors was based on variations in the sample air flow rate of $\pm 10\%$.

To determine the uncertainty associated with calculated values of the scattering and backscattering coefficients, input parameters were varied independently during a series of model runs. The parameters included the aerosol chemical composition, the RH and temperature of the sampled air stream, and the aerosol growth factor. The chemical composition, RH, and temperature affect the calculated aerosol density and refractive index. The aerosol growth factor refers to the change in particle size with an increase in RH due to the uptake of water [*Rood et al.,* 1987; *Berg et al.,* this issue]. It determines the degree to which the DMPS diameters (at 10% RH) were shifted so that they align with the APS diameters (at 30 to 45% RH). As discussed in section 2.1.3, constant growth factors of 1.2 for sulfate and 1.5 for sea-salt aerosol were used to shift the DMPS diameters. Each of these parameters affects the magnitude of scattering and backscattering by the aerosol as well as the conversion of the number distribution to a mass distribution for the estimation of total aerosol mass.

Since OptiClos depends on output from AeRho (see Figure 4), the model runs first were performed with AeRho. A total of four model runs were conducted with one input parameter being varied while the remaining were held constant. The amount that a parameter was allowed to vary was based on the range of measured values for each. Specifically, the chemical composition was varied by $\pm 2\%$ per ionic species per stage, RH was varied by $\pm 20\%$, and T was varied by $\pm 10\%$. The variation of temperature and RH was combined in one model run to test the largest range of water vapor possible.

The range of density and refractive index values from the sensitivity analyses of AeRho was used as input to OptiClos to determine the overall effect on calculated scattering and backscattering coefficients and total aerosol mass. Again, one input parameter was allowed to vary while the others were held constant. The only difference in this case was that six model runs were needed due to the addition of the nss $SO_4^=$ and sea-salt growth factors. These values were varied by $\pm 5\%$ which was the range of variation observed by *Berg et al.* [this issue] during ACE 1.

The derivation of both submicron and supermicron mass from the number size distribution was relatively insensitive to variations in chemical composition. This is to be expected given the simplicity of the measured composition, the relatively similar hygroscopicity and density of nss $SO_4^=$ and sea salt, and the assumption of an externally mixed aerosol. The derivation of submicron and supermicron mass was more sensitive to variations in RH. An increase in RH results in an increase in the aerosol water content and a decrease in particle density. This, in turn, leads to a decrease in the calculated mass concentration through the relation

$$\frac{dm}{d\log D_p} = \frac{dV}{d\log D_p}\rho \tag{10}$$

where $dV/d\log D_p$ is the particle volume size distribution calculated from the measured number distribution and ρ is the particle density. For the supermicron size

Table 3. Sources of Uncertainty in the Scattering and Backscattering Closure Experiments for a Wavelength of 0.55 μm

Method, M_i	Source of Uncertainty, p_i	δp_i,[a] %	δy_{Mi},[b] %
Integrating nephelometer			
σ_{sp_M},[c] submicron aerosol	calibration[d]		±8.8
	literature values	±1.2	
	gas density	±0.5	
	photon counting[d]		
	measurement and zero	±0.8	
	calibration	±0.4	
	RH control	±5.0	
	size cut	±7.1	
σ_{sp_M}, supermicron aerosol	calibration[d]		−11, +15
	literature values	±1.2	
	gas density	±0.5	
	photon counting[d]		
	measurement and zero	±0.8	
	calibration	±0.4	
	RH control	±5.0	
	size cut	±5.4	
	inlet losses	+10.0	
Integrating nephelometer			
σ_{bsp_M},[c] submicron aerosol	calibration[d]		±12
	literature values	±6.0	
	gas density	±2.5	
	photon counting[d]		
	measurement and zero	±5.5	
	calibration	±2.0	
	RH control	±5.0	
	size cut	±7.1	
σ_{bsp_M}, supermicron aerosol	Calibration[d]		−11, +15
	literature values	±6.0	
	gas density	±2.5	
	photon counting[d]		
	measurement and zero	±5.5	
	calibration	±2.0	
	RH control	±5.0	
	size cut	±5.4	
	inlet losses	+10.0	
Mie scattering model			
σ_{sp_T},[e] submicron aerosol	number distribution		−14, +17
	instrumental sizing	±2.5	
	instrumental counting	±10	
	calculation of σ_{sp_T} from OptiClos	−10, +13	
	which includes		
	chemical composition[f]	−0.07, +0.02	
	RH and T[g]	−6.1, +5.6	
	growth factor[h]	−7.8, +12	
σ_{sp_T}, supermicron aerosol	number distribution		−5, +20
	instrumental sizing	negligible	
	instrumental counting	±1.0	
	inlet losses	+20	
	calculation of σ_{sp_T} from OptiClos	−5, +1.5	
	which includes		
	chemical composition[f]	−0.9, +0.2	
	RH and T[g]	−1.9, +0.07	
	growth factor[h]	−4.7, +1.4	

Table 3. (continued)

Method, M_i	Source of Uncertainty, p_i	δp_i,[a] %	δy_{M_i},[b] %
Mie scattering model			
σ_{bsp_T},[e] submicron aerosol	number distribution		−17, +19
	instrumental sizing	±2.5	
	instrumental counting	±10	
	calculation of σ_{sp_T} from OptiClos which includes	−9.8, +12	
	chemical composition[f]	−2.3, +0.12	
	RH and T[g]	−6.4, +4.7	
	growth factor[h]	−7.1, +11	
σ_{bsp_T}, supermicron aerosol	number distribution		−6.4, +20
	instrumental sizing	negligible	
	instrumental counting	±1.0	
	inlet losses	+20	
	calculation of σ_{sp_T} from OptiClos which includes	−6.5, +3.5	
	chemical composition[f]	−0.1, +0.02	
	RH and T[g]	−5.6, +0.03	
	growth factor[h]	−3.4, +3.5	
Mie scattering model			
σ_{sp_Nsim},[i] submicron aerosol	angular nonidealities[d]	−0.1	±17
	wavelength nonidealities[d]	±0.02	
	number distribution		
	instrumental sizing	±2.5	
	instrumental counting	±10	
	calculation of σ_{sp_T} from OptiClos which includes	−9.5, +13	
	chemical composition[f]	−0.075, +1.7	
	RH and T[g]	−5.7, +5.4	
	growth factor[h]	−7.5, +11	
σ_{sp_Nsim},[i] supermicron aerosol	angular nonidealities[d]	−0.1	−21, +20
	wavelength nonidealities[d]	±0.02	
	number distribution		
	instrumental sizing	negligible	
	instrumental counting	±1.0	
	inlet losses	+20	
	calculation of σ_{sp_T} from OptiClos which includes	−6.1, +2.2	
	chemical composition[f]	−0.084, +0.13	
	RH and T[g]	−3.1, +1.0	
	growth factor[h]	−5.2, +2.2	
Mie scattering model			
σ_{bsp_Nsim},[i] submicron aerosol	angular nonidealities[d]	−0.1	−17, +16
	wavelength nonidealities[d]	±0.02	
	number distribution		
	instrumental sizing	±2.5	
	instrumental counting	±10	
	calculation of σ_{sp_T} from OptiClos which includes	−9.3, +12	
	chemical composition[f]	−2.0, +0.1	
	RH and T[g]	−6.1, +4.4	
	growth factor[h]	−6.7, +11	

Table 3. (continued)

Method, M_i	Source of Uncertainty, p_i	δp_i,[a] %	δy_{M_i},[b] %
σ_{bsp_Nsim},[i] supermicron aerosol	angular nonidealities[d]	−0.1	−12, +21
	wavelength nonidealities[d]	±0.02	
	number distribution		
	instrumental sizing	negligible	
	instrumental counting	±1.0	
	inlet losses	+20	
	calculation of σ_{sp_T} from OptiClos which includes	−6.7, +5.1	
	chemical composition[f]	−0.08, +0.2	
	RH and T[g]	−5.4, +1.0	
	growth factor[h]	−4.0, +5.1	

[a]Relative uncertainty of parameter p_i as defined by equation (8).
[b]Total relative uncertainty associated with method M_i calculated from equation (7). Sources of error are assumed to be independent. As such, the total error may be an underestimate.
[c]Here, σ_{sp_M} and σ_{bsp_M} are nephelometer-measured scattering and backscattering coefficients.
[d]Based on *Anderson et al.* [1996]; assumes $\sigma_{sp} = 20$ Mm^{-1} and $\sigma_{bsp} = 2$ Mm^{-1} and a 60 s measurement time.
[e]Here, σ_{sp_T} and σ_{bsp_T} are true scattering and backscattering coefficients based on equation (4).
[f]Chemical composition varied by 2% per chemical species per stage.
[g]RH varied by ±20% and temperature by ±10%.
[h]Growth factor varied by 1.2 ± 5% for nss $SO_4^=$ and 1.5 ± 5% for sea-salt aerosol [*Berg et al.*, this issue].
[i]Here, σ_{sp_Nsim} and σ_{bsp_Nsim} are nephelometer-simulated scattering and backscattering coefficients based on equation (6).

range, the decrease in particle density has a competing effect on the calculated mass concentration. The APS diameters are converted from aerodynamic to geometric by dividing by the square root of the particle density. As RH increases and density decreases, the shift from aerodynamic to geometric diameters becomes less dramatic resulting in larger geometric diameters. This results in a larger mass concentration when integrated over the supermicron size range.

The submicron, but not supermicron, calculated mass concentration also is sensitive to the aerosol growth factor. This results from the use of the growth factor to shift the DMPS diameters measured at 10% RH to align with those of the APS which were measured at 30 to 45% RH. The shift results in an increase in the mass concentration.

Similar results were seen for the sensitivity of the calculated scattering and backscattering coefficients to variations in model input parameters. Scattering and backscattering coefficients in both size ranges were relatively insensitive to changes in the chemical composition. Again, this is due to similarities in the hygroscopicity and refractive index of the nss $SO_4^=$ and sea-salt aerosol components as well as the assumption of an external mixture. Both the submicron and supermicron calculated coefficients are sensitive to variations in RH due to the effects on density described above. As RH increases, the aerosol water content and therefore density decreases. This results in a decrease in scattering. Changes in density have a second effect in the supermicron size range as it is used to shift APS diameters from aerodynamic to geometric. The density affects the degree of the shift and therefore the extent to which the supermicron aerosol is shifted down to the size range more efficient for scattering (≈0.2 to 1.0 μm). Similarly, sensitivity of the submicron aerosol to the growth factor results from the shift of the DMPS diameters, and therefore submicron mass, into the size range more efficient for scattering.

4. Results

4.1. Mass Closure

A comparison of the absolute values of the mass derived from IC and GA is shown in Figure 5. Mass derived from GA includes the water associated with the aerosol at 33% RH. In this figure, the IC mass has been partitioned into the mass of the ionic species and the mass of water associated with the aerosol at 33% RH as predicted by AeRho. The absolute values of the mass derived from all three methods (GA, IC, and ND) are shown in Figure 6. In both Figures 6 and 7, the uncertainty associated with each method is indicated by the error bars.

To evaluate closure, the mass derived from the IC and ND methods each were compared to that from the GA

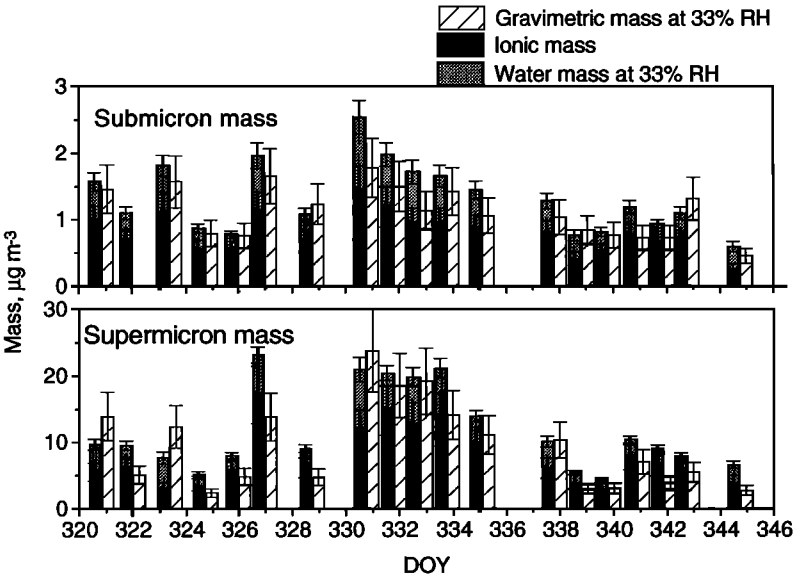

Figure 5. Absolute values of the submicron and supermicron aerosol mass concentration derived from gravimetric analysis (GA) and ion chromatography (IC). Mass derived from GA includes the amount of water associated with the aerosol at 33% RH. Mass derived from IC is partitioned into the water mass associated with the aerosol at 33% RH as predicted by AeRho and the mass of ionic species measured by ion chromatography. Also shown are the uncertainties associated with each method based on the information in Table 2.

method. The relative difference between methods was calculated using

$$\text{relative difference} = \left(\frac{m_{Mi} - m_{\text{GA}}}{m_{\text{GA}}}\right) \tag{11}$$

where m_{Mi} is the mass derived from IC or ND and m_{GA} is the mass derived from GA . The experimental uncertainty associated with the mass closure also was calculated in terms of the comparison of IC and GA or ND and GA such that

$$\text{experimental uncertainty} = \frac{\left[(\delta y_{Mi})^2 + (\delta y_{\text{GA}})^2\right]^{1/2}}{m_{\text{GA}}} \tag{12}$$

where δy_{Mi} refers to the uncertainty of IC or ND and δy_{GA} is the uncertainty of GA. The average and range of

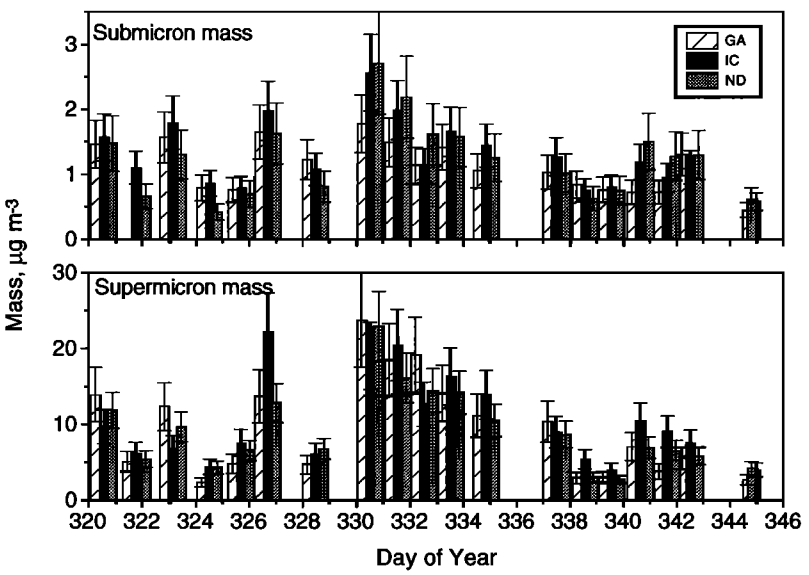

Figure 6. Absolute values of the submicron and supermicron aerosol mass concentration derived from gravimetric analysis (GA), ion chromatography (IC), and the number size distribution (ND). Mass derived from GA includes the amount of water associated with the aerosol at 33% RH. Mass derived from IC and ND includes the water mass at 33% RH as predicted by AeRho. Also shown are the uncertainties associated with each method based on the information in Table 2.

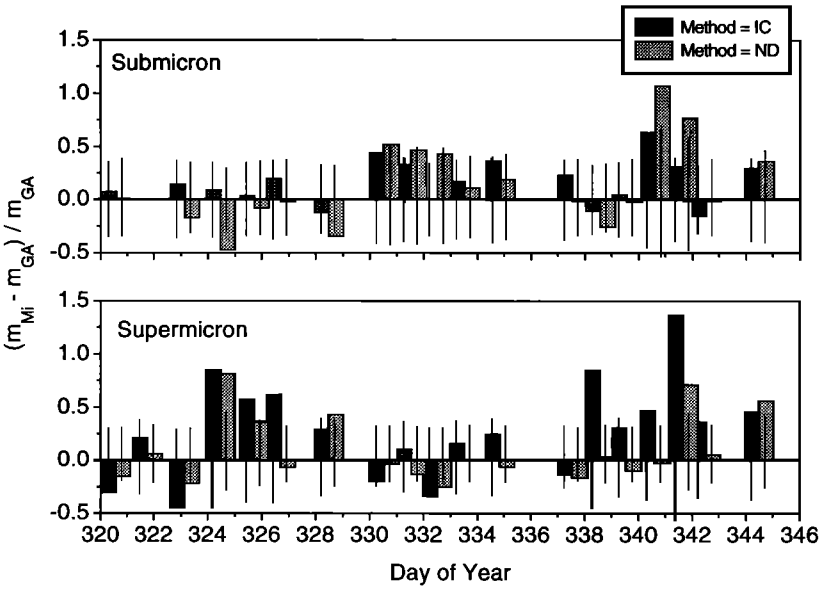

Figure 7. The shaded bars indicate the relative difference between the mass derived from ion chromatography (IC) and gravimetric analysis (dark bars) and between that derived from the number size distribution (ND) and gravimetric analysis (light bars). Relative difference is defined as $(m_{Mi}-m_{GA})/m_{GA}$ where m_{Mi} is the mass derived from IC or ND and m_{GA} is the mass derived from GA. The vertical lines indicate the experimental uncertainty associated with each sample. Experimental uncertainty is defined as $\left[(\delta y_{Mi})^2 + (\delta y_{GA})^2\right]^{1/2} / m_{GA}$.

the relative difference and the experimental uncertainty for all of ACE 1 are listed in Table 4. In addition, the relative difference and experimental uncertainty for each sample are compared in Figure 7.

For the submicron aerosol, the average relative difference between IC and GA mass was +10%, and between ND and GA, mass was +14%, while the experimental uncertainty was about ±40%. Thus the average relative difference in both cases was within the average experimental uncertainty. This degree of agreement between the IC and GA mass indicates that within the experimental uncertainty, essentially all of the submi-

Table 4. Mass Closure Results, Average Relative Difference Between the Mass Derived From Ion Chromatography (IC) and Gravimetric Analysis (GA) and Between That Derived From the Number Size Distribution (ND) and Gravimetric Analysis, and the Range of Relative Differences and the Average and Range of the Total Experimental Uncertainty

	Submicron, $D_p < 1.0$ μm		Supermicron, $1.0 \leq D_p < 10$ μm	
	IC	ND	IC	ND
Average relative difference,[a] %	+10	+14	+29	+3.4
Range of relative difference, %	−100 to 64	−100 to 120	−44 to 140	−46 to 206
Average experimental uncertainty[b]				
$-\delta y$, %	−37	−37	−34	−22
$+\delta y$, %	+37	+42	+40	+34
Range of experimental uncertainty, $\pm\delta y$, %	−45 to 45	−54 to 65	−57 to 60	−28 to 44

Results are presented for both the submicron and supermicron aerosol.

[a]Percent average relative difference equal to average of $(m_{M_i} - m_{GA})/m_{GA}$ where m_{M_i} refers to the IC or ND mass and m_{GA} is the mass derived from gravimetric analysis.

[b]Percent average experimental uncertainty equal to $\left[(\delta y_{M_i})^2 + (\delta y_{GA})^2\right]^{1/2} / m_{GA}$.

cron mass was ionic and was composed of those ions measured by the ion chromatography analysis plus the associated water mass.

The systematically higher values for both IC and ND relative to GA most likely are a result of the overestimation of the aerosol water mass from AeRho. In general, IC mass was less than GA mass but the addition of water to the IC mass led to values larger than the GA mass (Figure 5), indicating that too much water was added. The overprediction of water could be due to the use of a crystallization RH for sea salt that is too low (25%) such that an overabundance of water is associated with the sea-salt aerosol component except when the instrumental RH is at or lower than 25%. Recent results by *Tang et al.* [1997] indicate that a sea-salt solid phase may form nearer to 45% RH. The over-prediction also may result from the assumption of an externally mixed aerosol which precludes the reaction of nss $SO_4^=$ with Na^+ to form Na_2SO_4. Na_2SO_4 crystallizes at an RH of 59%, which is higher than the instrumental RH during ACE 1 of 30 to 45%. Therefore, if the aerosol was internally mixed, it is likely that solid Na_2SO_4 was present at the instrumental RH, which would result in a lower water mass concentration than was predicted by AeRho. Indeed, in cases where the submicron sea salt and nss $SO_4^=$ concentrations were high (DOY 330 to 334 and 340 to 341), the relative difference was the largest.

Assessing to what degree the predicted water mass was overestimated is not trivial, however, due to the difficulty in directly measuring it. The water mass associated with the aerosol as indicated by GA is not a direct measure due to potential interactions with the sampling substrate [*McInnes et al.*, 1996].

For the supermicron aerosol, the average relative difference between IC and GA mass was +29% and between ND and GA mass was +3.4% which was within experimental uncertainty. Again, the systematically higher values of the IC and ND mass relative to the GA mass could be due to the overprediction of water. For the supermicron aerosol, however, this cannot be a result of the assumption of an external mixture since 99% of the aerosol in this size range was sea salt [*Quinn et al.*, this issue]. Another factor, also related to the predicted aerosol water content, may contribute to the higher values of ND mass in this size range. A higher predicted aerosol water mass yields a lower predicted density. This affects the conversion of APS diameters from aerodynamic to geometric values. The overestimated water mass and resulting lower density results in less of a diameter shift and larger calculated mass concentrations.

The more sporadic relative differences seen for the supermicron size range could be a result of the difficulty of sampling large particles with a uniform collection efficiency. Although attempts were made to configure all instrument inlets uniformly, remaining differences could have led to differences in the amount of supermicron mass that was detected by the impactors versus the APS.

4.2. Scattering Closure

A comparison of the absolute values of the Mie-calculated true (T), nephelometer simulated (Nsim), and measured (M) scattering coefficients for the submicron and supermicron aerosol is shown in Figure 8. For evaluation of the scattering closure, the T and Nsim values each were compared to the measured values. Using equations similar to (11) and (12), the relative difference and experimental uncertainty were calculated between T and M and between Nsim and M. The average and

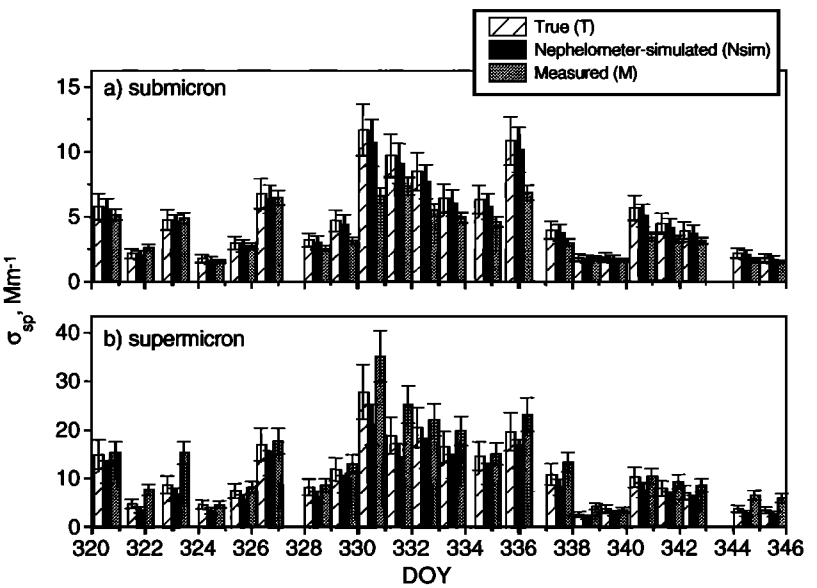

Figure 8. Absolute values of the (a) submicron and (b) supermicron Mie-calculated true scattering coefficient (T), nephelometer-simulated scattering coefficient (Nsim), and nephelometer-measured scattering coefficient (M). Error bars indicate the uncertainty associated with each method based on the information in Table 3.

range of the relative difference and experimental uncertainty are listed in Table 5. Values for each sampling period are shown in Figure 9.

For the submicron aerosol, T was systematically higher than M with an average relative difference of +28%. Nsim also was systematically higher than M with an average relative difference of +19%. This is within the range of experimental uncertainty of ±29%. The higher values of T relative to M are expected due to the angular truncation and wavelength errors of the nephelometer. Modifying the Mie integral to take into account nephelometer nonidealities should result in agreement between Nsim and M if Mie theory accurately describes the sampled aerosol and the nephelometer nonidealities are well-characterized.

Model calculations by *Anderson et al.* [1996] indicate that the ratio of nephelometer-simulated scattering to Mie-calculated true scattering is about 0.9 for diameters near 0.2 μm (for a lognormal distribution, geometric standard deviation of 2, and particle refractive index of 1.45). The ratio of Nsim to T for the submicron aerosol sampled during ACE 1 averaged 0.9, which is in good agreement with this calculated result. The ratio of M to T was lower, however, averaging 0.8. Thus, even though the relative difference between Nsim and M is within experimental uncertainty, there is a systematic difference between the two methods that needs to be explained.

The growth factor used to shift the DMPS diameters so that they align with the APS diameters may have contributed to the difference. If the average value of 1.2 for nss sulfate was too large for a given sampling period, then too much submicron nss $SO_4^=$ would be shifted more into the optically active size range. Hence the calculated submicron scattering values would be larger than those that were measured. This is supported by the correspondence between time periods of a large relative difference between Nsim and M and a

Table 5. Scattering and Backscattering Closure Results, Average Relative Difference Between the Nephelometer-Simulated Values (Nsim) and the Measured Values (M) and Between The Mie-Calculated True Values (T) and the Measured Values, and the Range of Relative Differences and the Average and Range of the Experimental Uncertainty for Each Comparison

	Submicron, $D_p < 1.0$ μm		Supermicron, $1.0 \leq D_p < 10$ μm	
	Nsim	True	Nsim	True
	Scattering Coefficient			
Average relative difference,[a] %	+19	+28	−37	−16
Range of relative difference, %	−22 to 61	−17 to 76	−56 to −19	−43 to 7.7
Average experimental uncertainty[b]				
$-\delta y$, %	−22	−20	−17	−12
$+\delta y$, %	+22	+23	+20	+22
Range of experimental uncertainty, $\pm\delta y$, %	−29 to 29	−26 to 31	−20 to 22	−12 to 26
	Backscattering Coefficient			
Average relative difference,[a] %	−8.2	−12	−42	−40
Range of relative difference, %	−36 to 26	−39 to 26	−59 to −27	−57 to −25
Average experimental uncertainty[b]				
$-\delta y$, %	−20	−19	−13	−12
$+\delta y$, %	+20	+21	+20	+20
Range of experimental uncertainty, $\pm\delta y$, %	−25 to 23	−24 to 26	−14 to 21	−12 to 21

[a]Percent average relative difference equal to average of $(\sigma_{sp\_Mi} - \sigma_{sp\_M})/\sigma_{sp\_M}$ where σ_{sp_Mi} is the scattering coefficient derived from the unmodified Mie calculation (σ_{sp_T}) or from the Mie calculation modified to simulate the nephelometer response (σ_{sp_Nsim}) and σ_{sp_M} is the measured value.

[b]Percent average experimental uncertainty equal to $\left[(\delta y_{Mi})^2 + (\delta y_M)^2\right]^{1/2}/\sigma_{sp\_M}$ where M_i = Nsim or T.

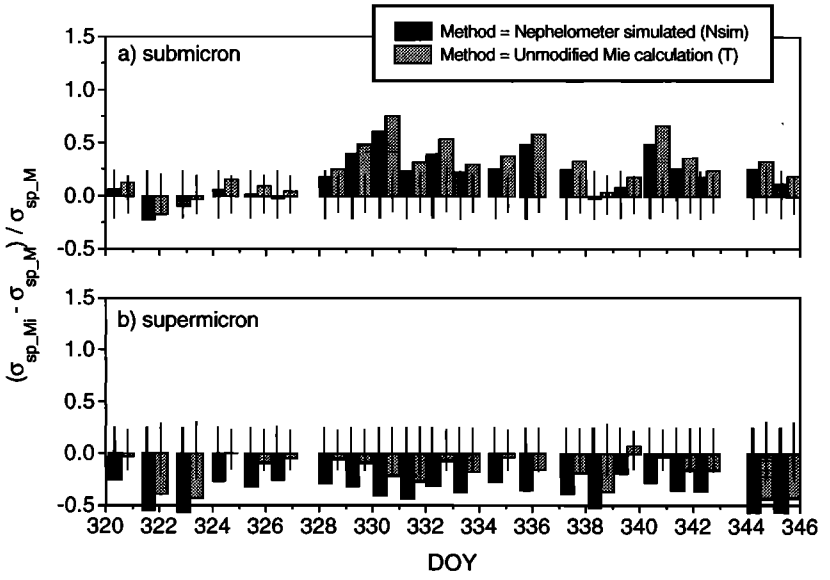

Figure 9. The shaded bars indicate the (a) submicron and (b) supermicron relative difference between the nephelometer-simulated (Nsim) and measured scattering coefficient (M) (dark bars) and between the Mie-calculated true (T) and measured scattering coefficient (M) (light bars). Relative difference is defined as $(\sigma_{sp\_Mi} - \sigma_{sp\_M})/\sigma_{sp\_M}$ where $\sigma_{sp\_Mi} = \sigma_{sp\_Nsim}$ or σ_{sp_T}. The error bars indicate the experimental uncertainty associated with each sample where experimental uncertainty is defined as $\left[(\delta y_{Mi})^2 + (\delta y_M)^2\right]^{1/2} / \sigma_{sp\_M}$.

measured nss $SO_4^=$ growth factor lower than 1.2 (DOY 329.5, 330.5, 332.5, 336, and 340.6). In contrast, the relative difference is the lowest at the start of the experiment (DOY 320 to 327) when nss $SO_4^=$ growth factors hovered around the average value of 1.2.

A second potential source of error is the assumption of spherical particles that is required by the Mie calculation. Particles may not be perfectly spherical at the instrumental RH of 30 to 45%. Na_2SO_4 has a crystallization RH of 59% and may contribute to a solid phase within the particle at a lower RH. How this would affect the submicron scattering is difficult to quantify, however, since little is known about the effects of "slush" on the scattering phase function.

For the supermicron aerosol, the average relative difference between scattering values derived from T and M was −16%, and between Nsim and M, it was −37% which is outside of the range of experimental uncertainty. There are factors which severely affect the accuracy of both the calculated and measured values in this size range, making it difficult to assess the significance of the relative difference. Both the T and Nsim methods are affected by the truncation of the measured number size distribution at 5 μm (which was done to prevent interference from phantom counts at large diameters in the APS measurement). In most cases, this resulted in an underestimation of surface area and therefore scattering. Scattering coefficients derived from the nephelometer measurement also suffer in this size range. As particle size increases, the amount of scattering in the near-forward direction also increases. Since this region is not efficiently sensed by the nephelometer, measured supermicron scattering coefficients can be underestimated by 20 to 50% [*Anderson et al.*, 1996]. As a result, it is likely that both the calculated and measured values underestimate the scattering coefficient of supermicron aerosol.

Clearly, a better estimation of the actual scattering by supermicron particles is needed and may be derived from

$$\sigma_{sp\_actual} = \sigma_{sp\_M} \frac{\sigma_{sp\_T}}{\sigma_{sp\_Nsim}} \tag{13}$$

This allows for the preservation of the information derived from the nephelometer yet takes into account its nonideal behavior.

4.3. Backscattering Closure

The absolute values of the Mie-calculated true (T), nephelometer simulated (Nsim), and measured (M) backscattering coefficients for both the submicron and supermicron aerosol are shown in Figure 10. Just as for the scattering closure, the relative difference between T and M and between Nsim and M was calculated using an equation similar to (11). In addition, the experimental uncertainty for each comparison was calculated using an equation similar in form to (12). The average and range of the relative difference and experimental uncertainty are listed in Table 5. Values for each sampling period are shown in Figure 11.

For the submicron aerosol, the average relative difference between values derived from T and M was −12%, and between Nsim and M, it was −8.2%, which is within the range of experimental uncertainty. In this size range, the nephelometer nonidealities result in arti-

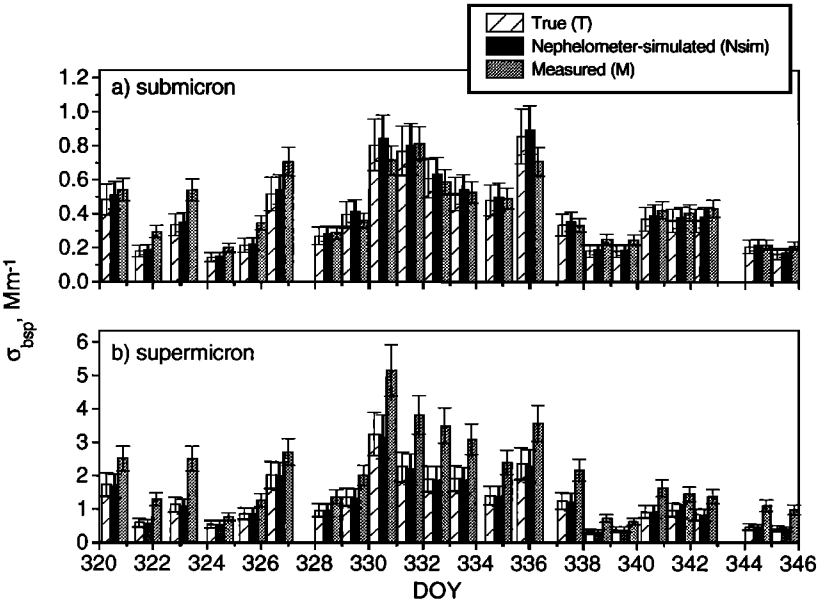

Figure 10. Absolute values of the (a) submicron and (b) supermicron Mie-calculated true backscattering coefficient (T), nephelometer-simulated backscattering coefficient (Nsim), and nephelometer-measured backscattering coefficient (M). Error bars indicate the uncertainty associated with each method based on the information in Table 3.

ficially high backscattering coefficients which undoubtedly helped improve the agreement between the calculated and measured values. *Anderson et al.* [1996] calculate a ratio of Nsim to T of about 1.05 to 1.08 for a diameter near 0.2 μm. The ACE 1 submicron average ratio of Nsim to T was 1.05, but the ratio of M to T was 1.18. Hence there is a systematic offset between the Mie-calculated true backscattering values and the measured values that is not explained by the nonidealities of the nephelometer response. The offset could be a result of the existence of a "slush" phase that was not taken into account in the model calculations and that cannot be accommodated by Mie theory.

The offset is more pronounced in the supermicron size range. Here the average relative difference between the T and M values was -40%, and between Nsim and M

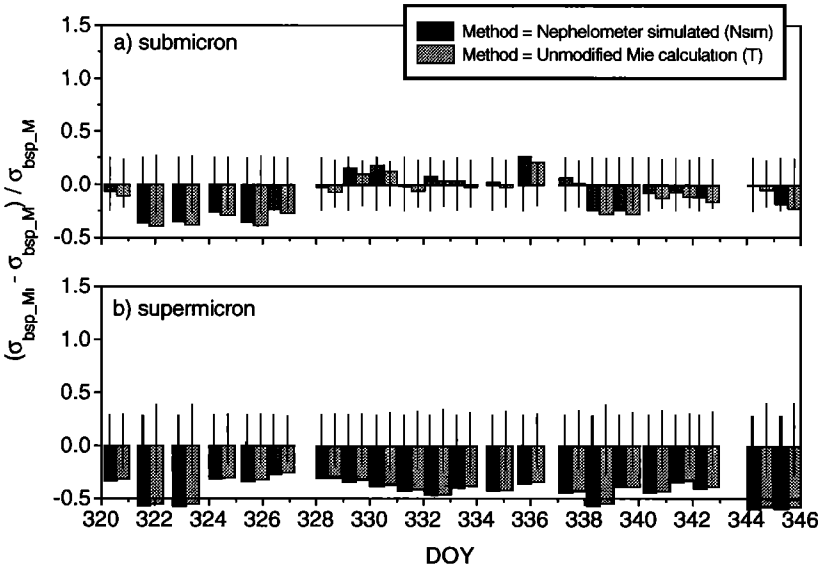

Figure 11. The shaded bars indicate the (a) submicron and (b) supermicron relative difference between the nephelometer-simulated (Nsim) and measured backscattering coefficient (M) (dark bars) and between the Mie-calculated true (T) and measured backscattering coefficient (M) (light bars). Relative difference is defined as $(\sigma_{\mathrm{bsp\_}Mi} - \sigma_{\mathrm{bsp\_}M})/\sigma_{\mathrm{bsp\_}M}$ where $\sigma_{\mathrm{bsp\_}Mi} = \sigma_{\mathrm{bsp\_Nsim}}$ or $\sigma_{\mathrm{bsp\_}T}$. The error bars indicate the experimental uncertainty associated with each sample where experimental uncertainty is defined as $[(\delta y_{Mi})^2 + (\delta y_M)^2]^{1/2}/\sigma_{\mathrm{bsp\_}M}$.

values it was −42%, which is outside of the range of experimental uncertainty of −14 to 21%. This discrepancy between calculated and measured values agrees with previous measurements of marine aerosol. *Quinn et al.* [1995] found that calculated backscattering coefficients for the total aerosol (submicron plus supermicron) were 40% lower than measured values for the tropical and NE Pacific Ocean. The truncation of the APS data at diameters larger than 5 μm most certainly contributes to this discrepancy. A better characterization of the coarse aerosol size distribution and backscattering behavior is needed to understand the factors contributing to this discrepancy.

5. Conclusions

Three methods of deriving the submicron and supermicron aerosol mass concentration were compared in a mass closure experiment. Concentrations of total aerosol mass were determined from gravimetric analysis and from a conversion of the measured number size distribution to a mass distribution. In addition, the concentration of water-soluble ionic species was determined from ion chromatography. For both size ranges, the average relative difference between the three methods was within experimental uncertainty. This indicates that within experimental uncertainty the aerosol mass was composed entirely of the ionic species measured by ion chromatography and the associated water mass.

Even though mass closure was obtained (average relative differences were within experimental uncertainty), discrepancies were observed between the three methods that deserve to be addressed. Mass values derived from ion chromatography and the number distribution were systematically higher than those derived from the gravimetric analysis. This difference most likely is a result of the overestimation of the aerosol water mass from the chemical equilibrium model which, in turn, is due to an incomplete understanding of the response of the aerosol to changes in relative humidity. A knowledge of the deliquescence and crystallization properties of the aerosol are needed for both the accumulation and coarse modes (where the majority of the aerosol mass resides and where scattering by particles is most efficient) and for a variety of aerosol types. In addition, there is a need to quantify the difference in the response of internally and externally mixed aerosols to RH changes.

Scattering and backscattering coefficients were determined from nephelometer measurements and a Mie scattering model. An unmodified Mie calculation was performed to derive the true scattering and backscattering coefficients. In addition, the Mie integral was modified to simulate the nephelometer response and calculate nephelometer-simulated scattering and backscattering coefficients. The relative difference between the scattering and backscattering coefficients derived from these three methods was within experimental uncertainty for the submicron aerosol. There was a systematic difference, however, between the calculated and measured values that was not accounted for by the simulation of the nephelometer nonidealities. This may be due to the assumption of spherical particles that is required by the Mie calculation but not met by the measurement at an RH of 30 to 45%. Again, a knowledge of the response of aerosol properties to changes in RH may help to determine the source of the systematic difference.

Closure was not achieved for scattering or backscattering for the supermicron aerosol. Measured scattering and, to a lesser extent, backscattering coefficients are underestimated by the nephelometer in this size range due to angular truncation errors. Accuracy of the calculated values is limited by uncertainties in the measurement and lognormal fitting of the number size distribution. The difference between calculated and measured values of the supermicron backscattering coefficient is similar to that previously reported for marine aerosol in the tropical and NE Pacific Ocean [*Quinn et al.*, 1995]. Instruments capable of accurately characterizing the size distribution and scattering properties of the coarse aerosol are needed to determine the source of this persistent difference.

During ACE 1, attempts were made to reduce the experimental uncertainty due to variations in RH by performing all measurements at a low, reference RH of 30 to 45%. Although the advantages of this approach are obvious, it does require that the characteristics and behavior of the aerosol at the lower RH be well understood. This includes understanding the phase transitions within the aerosol as it is exposed to a lower humidity and the resulting effects on the aerosol density, refractive index, and optical properties.

The thorough uncertainty analysis performed for all methods used in the mass and scattering closure experiments (see Tables 2 and 3) allows for the identification of those factors which make the largest contribution to the uncertainty associated with estimates of aerosol mass concentration and scattering and backscattering coefficients. On the basis of this analysis, reducing the uncertainty associated with aerosol mass concentration and scattering and backscattering coefficients should begin by focusing on the following:

1. Maintain the sample air flow that is supplied to all instruments at a uniform reference RH, thereby eliminating the need to correct for the effects of humidity differences between instruments and reducing errors associated with variations in RH. The value of the reference RH will depend on the aerosol chemical composition (i.e., volatility, prone to impactor bounce, etc.).

2. Characterize the aerosol water content as a function of chemical composition, RH, T, and mixing state. Studies based on single-particle levitation techniques [e.g., *Tang and Munkelwitz*, 1991, 1994; *Tang et al.*, 1997] have done much to advance the understanding of the effects of changing RH on particle water activity. In addition, humidity-controlled tandem differential

mobility analyzers (H-TDMA) [*Berg et al.*, this issue] reveal information about particle growth as a function of RH. These results can be used to improve model characterization of aerosol water content. In particular, they should be applied to the imposed condition of decreasing RH on the aerosol which is needed to establish the reference sampling RH. To date, the use of H-TDMAs has focused on particles with diameters less than 200 nm. Applying the method to larger particles would further our understanding of the response of these particles to changes in RH.

3. Minimize inlet losses of supermicron particles due to nonisokinetic flow. This involves the modeling of inlet losses as a function of inlet design and local wind conditions as well as empirical testing.

4. Characterize the coarse mode size distribution, preferably with a method that is insensitive to the particle refractive index to avoid calibration uncertainties.

5. Characterize the effect of changes in RH on scattering and backscattering by particles. Including dual nephelometers (one operating at the reference RH and one at a high RH (70 to 90%)), in a scattering closure experiment would provide useful information about the response of scattering to changes in RH [*Rood et al.*, 1987; K. Carrico et al., unpublished manuscript, 1997].

6. Characterize the effect of particle shape on scattering and backscattering by particles, particularly for the formation of a "slushy" particle as the RH of the sampled air is lowered to the reference RH. Information would be gained from laboratory experiments focused on the scattering and backscattering by different aerosol chemical compositions at a variety of humidities [*Quinn et al.*, 1996]. In addition, field measurements with a polar nephelometer would provide detailed information on the scattering intensity at a number of specific angles [*Waldram*, 1945].

The results of the closure experiments reported here have allowed an assessment of the ability of currently available techniques to accurately characterize the aerosol mass concentration and scattering and backscattering coefficients. Specifically, they have indicated areas of the measurement and modeling methods that are in need of improvement. Addressing these areas will lead to a reduction of the uncertainties associated with estimating aerosol mass and scattering properties.

Acknowledgments. We thank M. Hamilton, D. Hamilton, and J. Johnson for analytical and logistical assistance, D. Covert and T. Bates for helpful discussions, M. Laucks for Mie scattering efficiency tables, and the officers and crew of the *Discoverer* for their cooperation. This research was funded by the Aerosol Component of the NOAA Climate and Global Change Program. This research is a contribution to the International Global Atmospheric Chemistry (IGAC) Core project of the International Geosphere-Biosphere Programme (IGBP) and is part of the IGAC Aerosol Characterization Experiments (ACE). This is NOAA PMEL contribution 1863 and JISAO contribution 445.

References

Anderson, T. L., et al., Performance characteristics of a high-sensitivity, three-wavelength, total scatter/backscatter nephelometer, *J. Atmos. Oceanic Technol., 13*, 967–986, 1996.

Berg, O. H., E. R. Swietlicki, and R. Krejci, Hygroscopic growth of aerosol particles in the marine boundary layer over the Pacific and Southern Oceans during ACE 1, *J. Geophys. Res.*, this issue.

Berner, A., C. Lurzer, F. Pohl, O. Preining, and P. Wagner, The size distribution of the urban aerosol in Vienna, *Sci. Total Environ., 13*, 245–261, 1979.

Bohren, C. F., and D. R. Huffman, *Absorption and Scattering of Light by Small Particles*, John Wiley, New York, 1983.

Bray, W. H., Water vapor pressure control with aqueous solutions of sulfuric acid, *J. Mater. 5*, 233–248, 1970.

Bromley, L. A., Thermodynamic properties of strong electrolytes in aqueous solutions, *AIChE J., 19*, 313–320, 1973.

Covert, D. S., A. Wiedensohler, and L. M. Russell, Particle charging and transmission efficiencies of aerosol charge neutralizers, *Aerosol Sci. Technol., 27*, 206–214, 1997.

Heintzenberg, J., The angular calibration of the total scatter/backscatter nephelometer, consequences and applications, *Staub Reinhalt. Luft, 38*, 62–63, 1978.

Intergovernmental Panel on Climate Change (IPCC), *Climate Change 1995*, edited by J. T. Houghton et al., Cambridge Univ. Press, New York, 1996.

Marshall, S. F., Measurement-derived radiative transfer parameters for the aerosol climate forcing problem, M.S. dissertation, Univ. of Washington, Seattle, 1994.

Marshall, S. F., D. S. Covert, and R. J. Charlson, Relationship between asymmetry parameter and hemispheric backscatter ratio: Implications for climate forcing by aerosols, *Appl. Opt., 34*, 6306–6311, 1995.

McInnes, L. M., P. K. Quinn, D. S. Covert, and T. L. Anderson, Gravimetric analysis, ionic composition, and associated water mass of the marine aerosol, *Atmos. Environ., 30*, 869–884, 1996.

Murphy, D. M., J. R. Anderson, P. K. Quinn, L. M. McInnes, F. J. Brechtel, S. M. Kreidenweis, A. M. Middlebrook, M. Posfai, D. S. Thomson, and P. R. Buseck, Sea salt particles and aerosol radiative properties in the Southern Ocean marine boundary layer, *Nature*, in press, 1997.

O'Dowd, C. D., M. H. Smith, I. E. Consterdine, and J. A. Lowe, Marine aerosol, sea-salt, and the marine sulfur cycle: A short review, *Atmos. Environ., 31*, 73–80, 1997.

Pilinis, C., and J. H. Seinfeld, Continued development of a general equilibrium model for inorganic multicomponent atmospheric aerosols, *Atmos. Environ., 21*, 2453–2466, 1987.

Pitzer, K. S., and G. Mayorga, Thermodynamics of electrolytes, II, Activity and osmotic coefficients for strong electrolytes with one or both ions univalent, *J. Phys. Chem., 77*, 2300–2308, 1973.

Quinn, P. K., W. E. Asher, and R. J. Charlson, Equilibria of the marine multiphase ammonia system, *J. Atmos. Chem., 14*, 11–30, 1992.

Quinn, P. K., S. F. Marshall, T. S. Bates, D. S. Covert, and V. N. Kapustin, Comparison of measured and calculated aerosol properties relevant to the direct radiative forcing of tropospheric sulfate aerosol on climate, *J. Geophys. Res., 100*, 8977–8992, 1995.

Quinn, P. K., T. L. Anderson, T. S. Bates, R. Dlugi, J. Heintzenberg, W. von Hoyningen-Huene, M. Kulmala, P. B. Russell, and E. Swietlicki, Closure in tropospheric aerosol-climate research: A review and future needs for

addressing aerosol direct shortwave radiative forcing, *Beitr. Phys. Atmos., 69,* 547–577, 1996.

Quinn, P. K., D. J. Coffman, V. N. Kapustin, T. S. Bates, and D. S. Covert, Aerosol optical properties in the marine boundary layer during ACE 1 and the underlying chemical and physical aerosol properties, *J. Geophys. Res.,* this issue.

Robinson, R. A., and R. H. Stokes, *Electrolyte Solutions,* 2nd ed., Butterworths, London, 1965.

Rood, M. J., D. S. Covert, and T. V. Larson, Hygroscopic properties of atmospheric aerosol in Riverside, California, *Tellus, Ser. B., 39,* 383–397, 1987.

Rood, M. J., M. A. Shaw, T. V. Larson, and D. S. Covert, Ubiquitous nature of ambient metastable aerosol, *Nature, 337,* 537–539, 1989.

Stelson, A. W., Urban aerosol refractive index prediction by partial molar refraction approach, *Environ. Sci. Technol., 24,* 1676–1679, 1990.

Tang, I. N., and H. R. Munkelwitz, Simultaneous determination of refractive index and density of an evaporating aqueous solution droplet, *Aerosol Sci. Technol., 15,* 201–207, 1991.

Tang, I. N., and H. R. Munkelwitz, Water activities, densities, and refractive indices of aqueous sulfates and sodium nitrate droplets of atmospheric importance, *J. Geophys. Res., 99,* 18,801–18,808, 1994.

Tang, I. N., A. C. Tridico, and K. H. Fung, Thermodynamic and optical properties of sea-salt aerosols, *J. Geophys. Res., 102,* 23,269–23,275, 1997.

Waldram, J. M., Measurement of the photometric properties of the upper atmosphere, *Q. J. R. Meteorol. Soc., 71,* 319–336, 1945.

Whitby, E., and N. L. Whitby, DISTFIT computer program, TSI, Inc., St. Paul, Minn., 1989.

Wiedensohler, A., et al., Intercomparison study of the size-dependent counting efficiency of 26 condensation particle counters, *Aerosol Sci. Technol., 27,* 224–242, 1997.

Wiscombe, W. J., and G. W. Grams, The backscattered fraction in two-stream approximations, *J. Atmos. Sci., 33,* 2440–2451, 1976.

Young, J. F., Humidity control in the laboratory using salt-solutions—A review, *J. Appl. Chem., 17,* 241–245, 1967.

Zdanovskii, A. B., *Tr. Solyanoi Lab. Vses. Inst. Galurgii Akad. Nauk SSSR,* no. 6, 1936.

D. J. Coffman and P. K. Quinn, Pacific Marine Environmental Laboratory, NOAA, Seattle, WA 98115. (e-mail: quinn@pmel.noaa.gov; derek@pmel.noaa.gov)

(Received June 4, 1997; revised October 17, 1997; accepted December 23, 1997.)